

# Influence of geometric structure, convection, and eddy on sound propagation in acoustic metamaterial with turbulent flow

Myong Chol Pak\*, Kwang-Il Kim†, Hak Chol Pak‡, and Kwon Ryong Hong§  
*Kim Il Sung University, Taesong District, 136, Pyongyang, Democratic People's Republic of Korea*

The problem of reducing noise in the transportation is an important research field to prevent accidents and to provide a civilized environment for people. A material that has recently attracted attention in research to reduce noise is acoustic metamaterial, and most of the research projects so far have been limited to the case of static media without flow. We have studied the sound transmission properties of acoustic metamaterial with turbulent flow to develop acoustic metamaterial that be used in transportation. In this paper, the effect of geometrical structure, the convective effect, and the eddy effect on sound propagation in acoustic metamaterial with turbulent flow are investigated, and the relationships between them are analyzed. The convective effect and the eddy effect both reduce the resonant strength of sound transmission loss resulting from the unique geometry of the acoustic crystal, but shift the resonant frequencies in opposite directions. In addition, when the convective effect and the eddy effect of the airflow, as well as the intrinsic interaction effect generated from the unique geometrical structure of the acoustic metamaterial cannot be ignored, they exhibit competition phenomena with each other, resulting in a widening of the resonance peak. As a result, these three effects cause the shift of the resonance frequency of the sound transmission loss and the widening of the resonance peak. The results of this study show that even in the case of turbulent flow, acoustic metamaterial can be used for transportation by properly controlling the geometric size and shape of the acoustic metamaterial.

## Nomenclature

BLI	=	boundary-layer ingestion
CFD	=	computational field dynamics
$c_0$	=	Speed of sound, m/s
$k$	=	turbulent kinetic energy, $m^2/s^2$

---

\*Associate Professor, Department of Physics, Address/myongcholpak@163.com.

†Associate Professor, Department of Physics, Address/kwangilkim@163.com.

‡Professor, Department of Physics, Address/hcpak@163.com.

§Research fellow, Institute of Natural Sciences, Address/hongkwonryong@163.com.

$k_0$	=	wave number of incident acoustic wave, $m^{-1}$
LBM	=	lattice Boltzmann method
Ma	=	Mach number
$L_p$	=	sound pressure level, dB
PML	=	Perfectly Matched Layer
$p_{rms}$	=	root mean square pressure, Pa
$p_{ref}$	=	reference pressure for zero level corresponding to 0dB, Pa
RANS	=	Reynolds-averaged Navier-Stokes
$r_a$	=	radius of annular cavity, m
$r_d$	=	radius of circular duct, m
SPL	=	sound pressure level
SST	=	Shear Stress Transport
$t_a$	=	height of annular cavity, m
$t_d$	=	half of the height of neck in circular duct, m
TL	=	transmission loss, dB
$t_s$	=	height of acoustic source, m
$t_p$	=	height of PML, m
$\alpha_p$	=	coefficient of thermal expansion, $K^{-1}$
$\beta_T$	=	isothermal compressibility, $Pa^{-1}$
$\varepsilon$	=	turbulent dissipation rate, $m^2/s^3$
$\eta$	=	Kolmogorov's scale, m
$\mu$	=	dynamic viscosity, Pa·s
$\mu_B$	=	bulk viscosity, Pa·s
$\mu_T$	=	turbulent dynamic viscosity, Pa·s
$\nu$	=	fluid kinematic viscosity, $m^2/s$
$\nu_T$	=	turbulent kinematic viscosity, $m^2/s$
$\tau$	=	viscous stress tensor, Pa
$\tau_T$	=	turbulence time scale, s
$\omega$	=	specific dissipation rate, $s^{-1}$
$\omega_0$	=	angular frequency of incident acoustic wave, $s^{-1}$

## I. Introduction

WITH the recent development of technology, attentions been focused on the improvement of human environment, and interests in noise reduction are increasing. Among them, acoustic metamaterial are widely applied because they can reduce noise by controlling the density and the bulk modulus of the material.

Studies have been discussed using acoustic metamaterial to control sound transmission by absorbing low-frequency sound in linear and nonlinear regions [1, 2] and doping impurities inside zero-index metamaterial [3]. Also, the method for minimizing indoor sound energy by using an acoustic metamaterial with a flat panel structure [4] and the method for detecting an acoustic image by constructing an acoustic superlens using membrane-based a two-dimensional metamaterial having a negative density were reported [5]. In addition, a non-resonant metasurface design for broadband elastic wave mode division that be used for elastic communication and biomedical diagnostic evaluation has also been proposed [6]. Lu K. et al. showed through simulation that acoustic metamaterial with honeycomb structure effectively cause acoustic transmission loss in the low frequency range [7] and Fan L. et al. proved that the plates with circular holes blocked by membranes are effective in sound insulation at low frequencies by using numerical analysis [8]. Wang X. et al. proposed that a sound insulation effect can be obtained in the low frequency range by controlling the shape, stiffness and position of a thin film-type acoustic metamaterial with a stick fixed in the middle of the frame [9]. Acoustic metamaterial used to block broadband noise including low-frequency regions in air can be applied to water as well as air. Bok E. et al. proposed a way to use the acoustic metasurface consisting of a membrane and an air cavity filled with meta atoms in order to increase the acoustic sensitivity in water [10].

As the practical applicability of acoustic metamaterial increases, research projects on acoustic metamaterial panels that can increase the noise reduction function while passing through a fluid are actively taking place [11–13]. In Ref. [14], they designed an acoustic metamaterial panel that does not interfere with the flow of fluid while reducing the noise in a broadband in the audible frequency range. The proposed acoustic metamaterial panel allows the fluid to pass through the straight hole, but serves to block broadband noise by periodic annular cavities surrounding the hole. However, in these papers, the effect of the flow velocity of the fluid passing through the acoustic metamaterial on the sound wave is not discussed.

Meanwhile, research projects to control sound wave propagation in laminar and turbulent flows of fluids are also attracting attention. Yang Z. et al. proposed the idea that sound waves can propagate in one direction along the surface regardless of the presence of defects or obstacles in the acoustic structure with laminar circulation flow [15]. Research projects for investigating sound propagation properties in turbulent flow rather than laminar flow are attracting a lot of attention because they have a lot to do with practical applications. Turbulence effect of the fuselage on the fan noise of the BLI (Boundary-Layer Ingestion) configuration [16], the relationship between the structural flexibility of the elastic trailing-edge and the aeroacoustic response [17], prediction of broadband sound generated in a low Mach number turbulent boundary layer by lattice Boltzmann method (LBM) [18], simulation of indoor noise generated by indoor

window vibration [19], and acoustic source model to reduce aerodynamic noise generated from wind turbine blades [20] have been discussed. Most of the interest, such as the reduction of aerofoil interaction noise by new serration profile group [21, 22], the noise generation mechanism of controlled diffusion aerofoil and their dependence on Mach number [23], and the role of the porous material placed on the tail edge of the 3D chamber airfoil [24], focuses on the reduction of noise caused by the interaction between aerofoil and turbulent flow.

Most of the researchers are only interested in sound wave control and noise generation in turbulent flows, but there are few studies on the effect of geometric structure, convective, and eddy effect on sound propagation in acoustic metamaterial with turbulent flow. Therefore, we discuss the convective and eddy effects on acoustic propagation as turbulence flows into the acoustic metamaterial consisting of straight holes and periodic annular cavities surrounding the hole. Also, in this case, the change in broadband acoustic wave blocking characteristics according to the geometric size and the number of annular cavities is investigated. This paper is organized as follows. Section 2 describes the theoretical basis for aeroacoustic properties in turbulent flows. In Section 3, numerical results for sound transmission loss and sound pressure level of acoustic metamaterial are shown and analyzed in both cases of no flow and turbulent flow. In particular, the turbulence flowing in the acoustic metamaterial is analyzed by CFD (computational fluid dynamics), and based on the results, the convective effect and the eddy effect on sound transmission are discussed. Also, the sound transmission properties according to the geometric size of acoustic crystals and the number of ring-shaped cavities are also considered. Finally, in Section 4, the influence of geometric structure, convection, and eddy on sound propagation in acoustic metamaterial with turbulent flows are concluded, and future application prospects are described.

## II. Theoretical Background

Using the linearized Navier-Stokes equation, we study the propagation properties of sound waves in a fluid. This equation consists of the continuity, momentum, and energy equations [25].

$$\frac{\partial \rho_t}{\partial t} + \nabla \cdot (\rho_0 \mathbf{u}_t + \rho_t \mathbf{u}_0) = M \quad (1)$$

$$\rho_0 \left[ \frac{\partial \mathbf{u}_t}{\partial t} + (\mathbf{u}_t \cdot \nabla) \mathbf{u}_0 + (\mathbf{u}_0 \cdot \nabla) \mathbf{u}_t \right] + \rho_t (\mathbf{u}_0 \cdot \nabla) \mathbf{u}_0 = \nabla \cdot \boldsymbol{\sigma} + \mathbf{F} - \mathbf{u}_0 M \quad (2)$$

$$\rho_0 C_p \left[ \frac{\partial T_t}{\partial t} + (\mathbf{u}_t \cdot \nabla) T_0 + (\mathbf{u}_0 \cdot \nabla) T_t \right] + \rho_t C_p (\mathbf{u}_0 \cdot \nabla) T_0 \quad (3)$$

$$- \alpha_p T_0 \left[ \frac{\partial p_t}{\partial t} + (\mathbf{u}_t \cdot \nabla) p_0 + (\mathbf{u}_0 \cdot \nabla) p_t \right] - \alpha_p T_t (\mathbf{u}_0 \cdot \nabla) p_0 = \nabla \cdot (\kappa \nabla T_t) + \Phi + Q$$

where  $p_t$ ,  $\mathbf{u}_t$ ,  $T_t$ , and  $\rho_t$  are the acoustic perturbations to the pressure, the velocity, the temperature, and the density, respectively.  $p_t$ ,  $\mathbf{u}_t$ , and  $T_t$  are equal to the sum of the physical quantities in the background acoustic field and the scattered field.

$$p_t = p + p_b, \mathbf{u}_t = \mathbf{u} + \mathbf{u}_b, T_t = T + T_b \quad (4)$$

Also,  $M$ ,  $\mathbf{F}$ ,  $Q$ ,  $C_p$ ,  $\alpha_p$ , and  $\kappa$  are the mass source, the volume force source, the volumetric heat source, the heat capacity at constant pressure, the coefficient of thermal expansion, and the thermal conductivity, respectively. Additionally, the stress tensor, the linearized equation of state and the linearized viscous dissipation function are defined as,

$$\sigma = -p_t \mathbf{I} + \mu(\nabla \mathbf{u}_t + (\nabla \mathbf{u}_t)^T) + (\mu_B - 2\mu/3)(\nabla \cdot \mathbf{u}_t) \mathbf{I} \quad (5)$$

$$\rho_t = \rho_0(\beta_T p_t - \alpha_p T_t) \quad (6)$$

$$\Phi = \nabla \mathbf{u}_t : \tau(\mathbf{u}_0) + \nabla \mathbf{u}_0 : \tau(\mathbf{u}_t) \quad (7)$$

$$\tau(\mathbf{u}_t) = \mu[\nabla \mathbf{u}_t + (\nabla \mathbf{u}_t)^T] + (\mu_B - 2\mu/3)(\nabla \cdot \mathbf{u}_t) \mathbf{I} \quad (8)$$

$$\tau(\mathbf{u}_0) = \mu[\nabla \mathbf{u}_0 + (\nabla \mathbf{u}_0)^T] + (\mu_B - 2\mu/3)(\nabla \cdot \mathbf{u}_0) \mathbf{I} \quad (9)$$

where  $\tau$ ,  $\beta_T$ ,  $\mu$ , and  $\mu_B$  are the viscous stress tensor, the isothermal compressibility, the dynamic viscosity and the bulk viscosity, respectively. In the linearized Navier-Stokes equation,  $p_0$ ,  $\mathbf{u}_0$ ,  $T_0$ , and  $\rho_0$  are absolute pressure, velocity, temperature, and density of the background mean flow used to account for the effect of the background mean flow on the sound wave. This is calculated by using the CFD study of the fluid.

When sound waves propagate into a turbulent flow, the flow properties are evaluated by Reynolds-averaged Navier-Stokes (RANS) model [26]. The Reynolds-averaged representation of turbulent flows divides the flow quantities into a time-averaged part and a fluctuating part.

$$\mathbf{u}_0 = \bar{\mathbf{u}}_0 + \mathbf{u}'_0, \rho_0 = \bar{\rho}_0 + \rho'_0, p_0 = \bar{p}_0 + p'_0 \quad (10)$$

In order to discuss the turbulent flow, the SST (Shear Stress Transport) turbulent method is used among various RANS models [25]. The advantage of this method is that it can describe the flow characteristics well close to the wall and the dependence on the initial parameters of the main free stream flow is not very large.

The basic equation governed is as follows.

$$\frac{\partial \bar{\rho}_0}{\partial t} + \nabla \cdot (\bar{\rho}_0 \bar{\mathbf{u}}_0) = 0 \quad (11)$$

$$\begin{aligned} \bar{\rho}_0 \frac{\partial \bar{\mathbf{u}}_0}{\partial t} + \bar{\rho}_0 (\bar{\mathbf{u}}_0 \cdot \nabla) \bar{\mathbf{u}}_0 &= \nabla \cdot \{-\bar{\rho}_0 \mathbf{I} + (\mu + \mu_T) [\nabla \bar{\mathbf{u}}_0 + (\nabla \bar{\mathbf{u}}_0)^T] \\ &\quad - \frac{2}{3} (\mu + \mu_T) (\nabla \cdot \bar{\mathbf{u}}_0) \mathbf{I} - \frac{2}{3} \bar{\rho}_0 k \mathbf{I}\} + \mathbf{F} \end{aligned} \quad (12)$$

The model equations are formulated in the averaged turbulent kinetic energy  $k$  and the turbulent frequency  $\omega$ ,

$$\bar{\rho}_0 \frac{\partial k}{\partial t} + \bar{\rho}_0 (\bar{\mathbf{u}}_0 \cdot \nabla) k = \nabla \cdot [(\mu + \mu_T \sigma_k) \nabla k] + P - \bar{\rho}_0 \beta_0^* k \omega \quad (13)$$

$$\bar{\rho}_0 \frac{\partial \omega}{\partial t} + \bar{\rho}_0 (\bar{\mathbf{u}}_0 \cdot \nabla) \omega = \frac{\bar{\rho}_0 \gamma}{\mu_T} P - \bar{\rho}_0 \beta \omega^2 + \nabla \cdot [(\mu + \mu_T \sigma_\omega) \nabla \omega] + 2(1 - f_{v1}) \frac{\bar{\rho}_0 \sigma_\omega^2}{\omega} \nabla \omega \cdot \nabla k \quad (14)$$

where,

$$P = \min(P_k, 10 \bar{\rho}_0 \beta_0^* k \omega) \quad (15)$$

$$P_k = \mu_T \{ \nabla \bar{\mathbf{u}}_0 : [\nabla \bar{\mathbf{u}}_0 + (\nabla \bar{\mathbf{u}}_0)^T] - \frac{2}{3} (\nabla \cdot \bar{\mathbf{u}}_0)^2 \} - \frac{2}{3} \bar{\rho}_0 k \nabla \cdot \bar{\mathbf{u}}_0 \quad (16)$$

In this case, the turbulent eddy viscosity is,

$$\mu_T = \frac{\bar{\rho}_0 \alpha_1 k}{\max(\alpha_1 \omega, S f_{v2})} \quad (17)$$

where  $S$  is the characteristic magnitude of the mean velocity gradients,

$$S = \sqrt{2 S_{ij} S_{ij}} \quad (18)$$

and  $S_{ij}$  is the mean strain-rate tensor,

$$S_{ij} = \frac{1}{2} \left( \frac{\partial \bar{u}_{0i}}{\partial x_j} + \frac{\partial \bar{u}_{0j}}{\partial x_i} \right) \quad (19)$$

The constants  $\beta$ ,  $\gamma$ ,  $\sigma_k$ , and  $\sigma_\omega$  are interpolated values between inner and outer values.

$$\left\{ \begin{array}{l} \beta = f_{v1} \beta_1 + (1 - f_{v1}) \beta_2 \\ \gamma = f_{v1} \gamma_1 + (1 - f_{v1}) \gamma_2 \\ \sigma_k = f_{v1} \sigma_{k1} + (1 - f_{v1}) \sigma_{k2} \\ \sigma_\omega = f_{v1} \sigma_{\omega 1} + (1 - f_{v1}) \sigma_{\omega 2} \end{array} \right. \quad (20)$$

The interpolation functions  $f_{v1}$  and  $f_{v2}$  are

$$f_{v1} = \tanh(\theta_1^4) \quad (21)$$

and,

$$f_{v2} = \tanh(\theta_2^2). \quad (22)$$

In this case,

$$\theta_1 = \min\left[\max\left(\frac{\sqrt{k}}{\beta_0^* \omega l_\omega}, \frac{500\mu}{\bar{\rho}_0 \omega l_\omega^2}, \frac{4\bar{\rho}_0 \sigma_{\omega 2} k}{CD_{k\omega} l_\omega^2}\right)\right], \quad (23)$$

$$CD_{k\omega} = \max\left(\frac{2\bar{\rho}_0 \sigma_{\omega 2}}{\omega} \nabla \omega \cdot \nabla k, 10^{-10}\right), \quad (24)$$

$$\theta_2 = \max\left(\frac{2\sqrt{k}}{\beta_0^* \omega l_\omega}, \frac{500\mu}{\bar{\rho}_0 \omega l_\omega^2}\right). \quad (25)$$

where  $\beta_1 = 0.075$ ,  $\beta_2 = 0.0828$ ,  $\gamma_1 = 5/9$ ,  $\gamma_2 = 0.44$ ,  $\sigma_{k1} = 0.85$ ,  $\sigma_{k2} = 1$ ,  $\sigma_{\omega 1} = 0.5$ ,  $\sigma_{\omega 2} = 0.856$ ,  $\alpha_1 = 0.31$ ,  $\beta_0^* = 0.09$ , and  $l_\omega$  is the distance to the closest wall.

### III. Results and Analysis

In this section, we first describe the simulation parameters and acoustic characteristic parameters of the acoustic metamaterial to be considered. Also, in order to investigate the effect of the geometrical structure on sound transmission, sound pressure level characteristic values and transmission loss results are calculated and analyzed using finite element simulation in the case of no flow. Next, when there is turbulent flow, the CFD analysis of the flow is performed, and sound transmission properties are investigated for the flow velocity, and the convective effect and the eddy effect are compared with each other. Finally, while changing the geometric structure parameter, we observe the change of sound pressure level and sound transmission loss values.

#### A. Simulation parameters

Fig. 1 is a design diagram of an acoustic metamaterial consisting of a straight hole through which a fluid can pass and periodic annular cavities surrounding the hole. In Fig.1,  $r_a$  is the radius of annular cavity,  $r_d$  is the radius

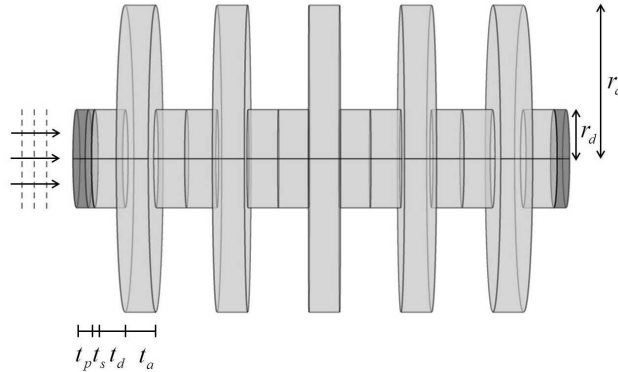


Fig. 1 A design diagram of the acoustic metamaterial to be discussed.

of circular duct,  $t_a$  is the height of annular cavity,  $t_d$  is a half of the height of neck in circular duct,  $t_s$  is the height of acoustic source, and  $t_p$  is the height of PML(Perfectly Matched Layer). Table 1 shows the remaining geometric structure parameter values excluding  $r_a$  because the calculation is performed while changing the size of the radius  $r_a$ .

**Table 1 Geometric structure parameters**

$r_d(\text{mm})$	$t_a(\text{mm})$	$t_d(\text{mm})$	$t_s(\text{mm})$	$t_p(\text{mm})$
8	5	5	1	2

As shown in Fig. 1, the discussed acoustic wave is a plane wave, and its incident surface is perpendicular to the rotation axis direction of the acoustic metamaterial. The finite element simulation was performed with the commercial software COMSOL Multiphysics 5.5. In this case, the boundary condition of the numerical simulation is assumed to be no slip and the sound velocity is  $c_0 = 343$  m/s. PML is applied at the inlet and outlet, which acts to absorb acoustic waves by simulating an open boundary. We calculated the sound pressure in the frequency range of 2000 to 6000 Hz and evaluated the transmission loss and sound pressure level based on it. In this case, the transmission loss of the system is defined as,

$$TL = 20\log_{10}\left(\left|\frac{p_{in}}{p_{out}}\right|\right) \quad (26)$$

where  $p_{in}$  and  $p_{out}$  are the average pressure at the inlet and outlet, respectively [27, 28]. And when the sound pressure  $p$  changes harmonically with time, the sound pressure level (SPL)  $L_p$  is expressed by the root mean square (rms) pressure  $p_{rms}$  of the fluid, such as

$$L_p = 20\log_{10}\left(\frac{p_{rms}}{p_{ref}}\right), \quad p_{rms} = \sqrt{pp^*/2} \quad (27)$$

where  $p_{ref}$  is the reference pressure for the zero level corresponding to 0dB [29]. The zero level corresponding to this dB scale depends on the type of fluid. For example, the reference pressure for air is  $20\mu\text{Pa}$  and the reference pressure for water is  $1\mu\text{Pa}$ .

## B. Calculation results of sound pressure level in case of no flow

We first investigate the acoustic pressure of the acoustic metamaterial in case of no flow in order to evaluate the effect of the geometry on the sound transmission of the acoustic metamaterial with turbulent flow. In this case, an incident acoustic plane wave with an amplitude of 1Pa is incident in a direction perpendicular to the axis of rotation of the acoustic metamaterial in the area marked in red in Fig. 1. Since the properties of the sound pressure vary according to the geometric size, we investigated the change in the sound pressure level corresponding to the radius of annular cavity and the number of annular cavities.

Fig. 2(a) shows the sound pressure level values versus the frequencies of the sound wave when there is no flow



( $Ma=0$ ) and the radius of annular cavity is 22.5mm. As shown in Fig. 2(a), as the frequency increases initially, the sound pressure level values decrease rapidly, have a minimum value at a specific frequency (4529.1 Hz in the case of  $N=5$ ), and then rise again. In other words, it has a resonant property, which can be treated as the result of the interaction between the particle vibration in the direction of sound propagation in the circular duct and the particle vibration perpendicular to the direction of sound propagation in the annular cavity [14].

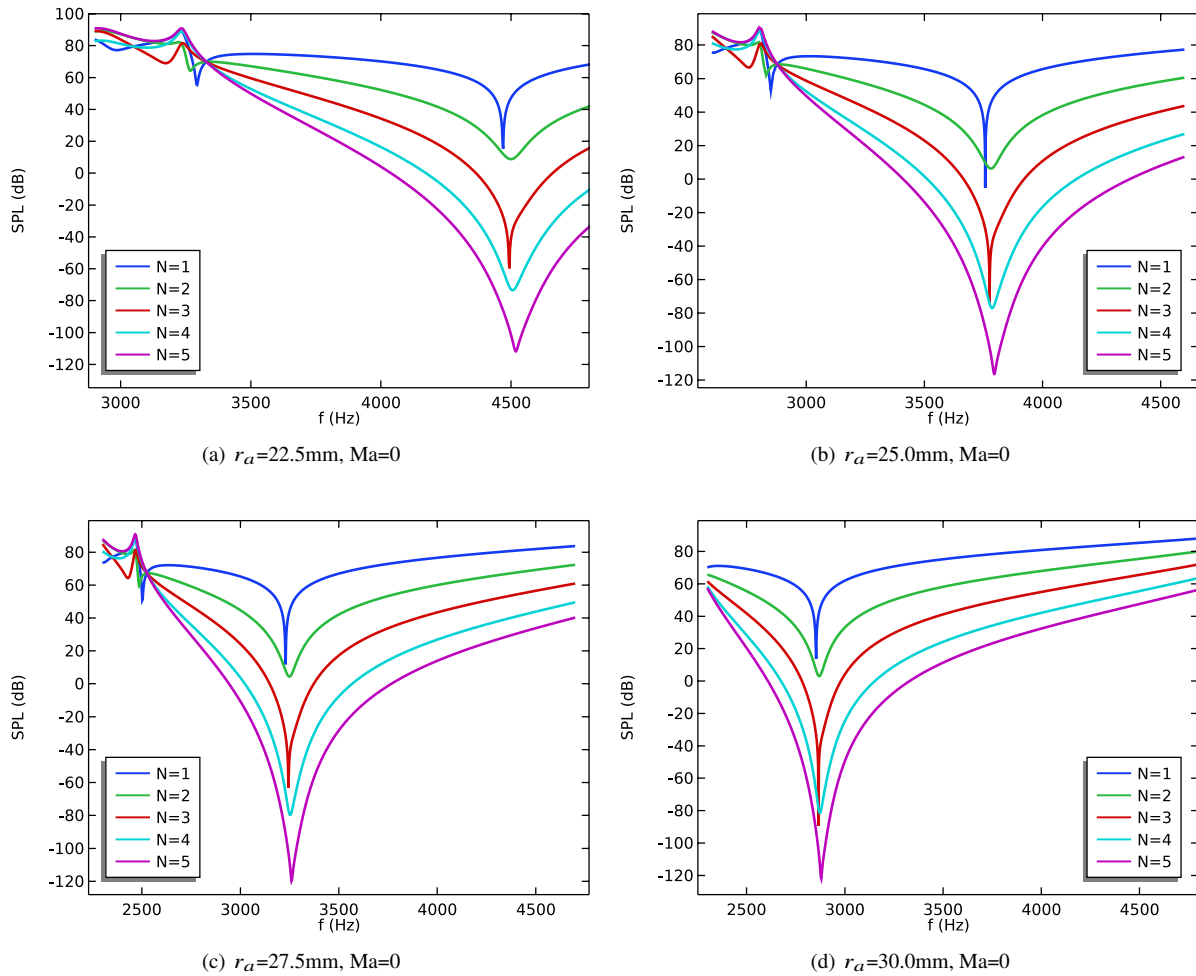


**Fig. 2** In the case of no flow, the change in sound pressure level according to the change in the radius of annular cavity and number of annular cavities.

This property appears regardless of the number of annular cavities. However, as the number increases, the magnitude of these minima becomes obviously smaller and the resonance strength becomes stronger. This is because, as the number of annular cavities increases, the cross-region between the particle vibration in the sound propagation direction in the circular duct and the particle vibration perpendicular to the sound propagation direction in the annular cavity increases, and as a result, the interaction becomes stronger. In the case of  $N=1$ , another peak appears at 3293.8Hz. Its peak intensity is smaller than the peak discussed earlier, and it gets weaker as the number of annular

cavities increases. This is a peak related to the length of the circular duct. In the case of  $N=1$ , this peak cannot be ignored because the resonance related to the interaction is not very large. However, as the number of annular cavities increases, the interaction between the particle vibration in the direction of sound propagation in the circular duct and the particle vibration perpendicular to the direction of sound propagation in the annular cavity increases, and the intensity of this peak disappears.

Even when  $r_a$  are 25.0mm, 27.5mm, and 30.0mm, the resonance properties analyzed above still appear (Fig. 2(b), 2(c), 2(d)). Table 2 shows the resonant frequency values corresponding to the annular cavity radii when  $N=5$ . Note in Fig. 2 and Table 2 that the resonant frequency decreases as the radius of the annular cavity increases. This is analyzed with particle vibrations perpendicular to the direction of sound propagation in the annular cavity. As the radius of the annular cavity increases, the wavelength of the stationary wave in the cavity increases, and thus the resonance frequency decreases. As a result, the resonance frequency of the sound propagation is also lowered due to the interaction between the particle vibration in the sound propagation direction in the circular duct and the particle vibration perpendicular to the sound propagation direction in the annular cavity. This proves once again that this resonance property is closely related to the particle vibration in the annular cavity.

**Table 2 Resonant frequency values corresponding to the radii of annular cavity in case of  $N=5$**

$r_a$ (mm)	22.5	25.0	27.5	30.0
$f^{res}$ (Hz)	4529.1	3804.8	3267.6	2862.3

### C. CFD analysis for turbulent flow

In order to investigate the sound propagation properties of acoustic metamaterial with turbulent flow, CFD analysis of turbulence in airflow is performed using the SST model mentioned above. The velocity of turbulent flow is evaluated with the Mach number  $Ma$ , and the properties of the case where  $Ma$  is 0.02, 0.05, 0.10, 0.15, 0.17, 0.20, 0.22 are discussed. In this case, the kinematic viscosity of air is  $\nu = 1.50 \times 10^{-5} \text{ m}^2/\text{s}$ .

To investigate turbulent flow, the turbulent kinetic energy  $k$ , specific dissipation rate  $\omega$ , turbulent dissipation rate  $\varepsilon$ , turbulent dynamic viscosity  $\mu_T$ , turbulent kinematic viscosity  $\nu_T$ , and turbulence time scale  $\tau_T$  should be evaluated and analyzed. Table 3 shows the turbulent flow parameters obtained at the outlet of the acoustic metamaterial by simulating while changing the velocity of the turbulent flow. As  $Ma$  increases, turbulent kinetic energy, specific dissipation rate, turbulent dissipation rate, turbulent dynamic viscosity, and turbulent kinematic viscosity increase. However, the turbulence time scale decreases as  $Ma$  increases, which is in good agreement with the fact that  $\tau_T$  is inversely proportional to the specific dissipation rate  $\omega$ . Fig. 3 shows a quarter cross section of turbulent dynamic viscosity  $\mu_T$  in the case of  $Ma = 0.15$ . It is evident that the turbulent dynamic viscosity is not zero in the annular cavity region of Fig.3, and this fact intuitively shows that the annular cavity region has a great influence on the airflow

flowing through the circular duct.

**Table 3** Turbulent flow parameters at the outlet of acoustic metamaterial

Ma	0.02	0.05	0.10	0.15	0.17	0.20	0.22
$k$ ( $\text{m}^2/\text{s}^2$ )	0.00538	0.225	3.86	14.6	21.1	33.3	43.0
$\omega$ ( $10^5\text{s}^{-1}$ )	8.92	8.94	9.25	10.1	10.5	11.3	11.9
$\varepsilon$ ( $10^4\text{m}^2/\text{s}^3$ )	0.0432	1.81	32.1	132	199	338	461
$\mu_T$ ( $10^{-7}\text{Pa} \cdot \text{s}$ )	0.0727	3.03	50.2	175	242	355	436
$\nu_T$ ( $10^{-7}\text{m}^2/\text{s}$ )	0.0603	2.52	41.7	145	201	294	361
$\tau_T$ ( $10^{-5}\text{s}$ )	1.25	1.24	1.20	1.11	1.06	0.983	0.933

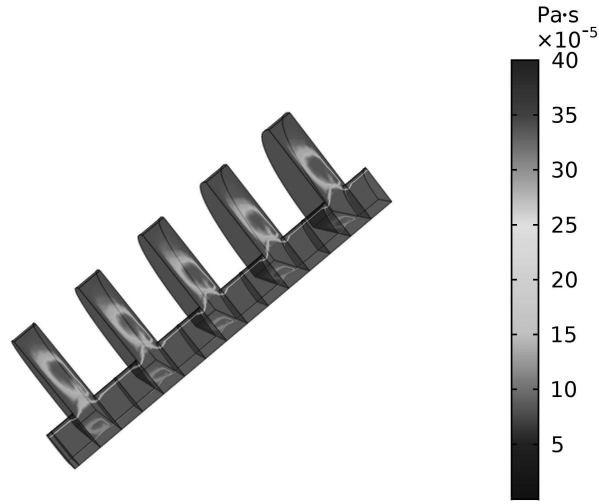


**Fig. 3** Quarter cross section of the turbulent dynamic viscosity in the case of Ma=0.15.

It is important to evaluate the property of the turbulent dissipation rate  $\varepsilon$  well in investigating the turbulent flow of a fluid. The turbulent dissipation rate  $\varepsilon$  does not depend on the kinematic viscosity  $\nu$ , but instead is determined by the nature of the largest eddy that extracts energy from the mean flow [30]. A scale that well reflects the balance between the inertia effect and the viscous effect of eddy is Kolmogorov's scale, defined as,

$$\eta = (\nu^3/\varepsilon)^{1/4} \quad (28)$$

Therefore, it is necessary to consider this scale carefully to evaluate the properties of turbulent flow and to analyze the sound transmission result accurately in turbulent flow. Thus, we investigated the Kolmogorov's scale versus the velocity of air (Fig. 4). As shown in Fig. 4, as Ma increases, Kolmogorov's scale gradually decreases. That is, the faster the velocity, the smaller the effect of eddy. In Fig. 4, the scale change was also investigated while changing the

number of annular cavities, but there is no significant change depending on the number.

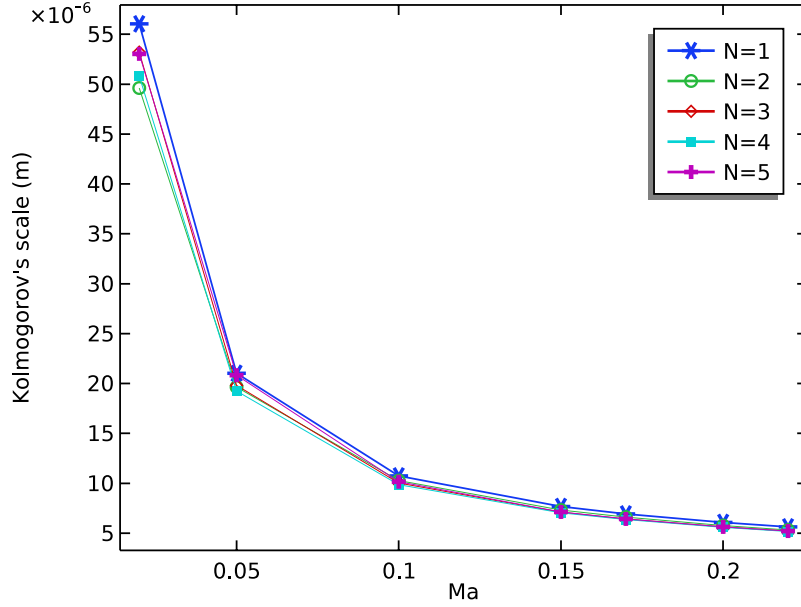


**Fig. 4** Kolmogorov's scale versus the velocity of airflow.

#### D. Sound transmission in turbulent flow

We investigated the transmission properties of sound waves in turbulent flow with the linearized Navier-Stokes Model discussed in Section 2, based on determining the pressure, velocity, temperature, and density of turbulent flow in acoustic metamaterial. In this case, the incident acoustic plane wave of  $p_b = p_0 e^{-ik_0 z}$  is incident on the area marked in red in Fig. 1 in a direction perpendicular to the rotation axis of the acoustic metamaterial, where  $p_0 = 1\text{Pa}$ ,  $k_0 = \omega_0 / [c_0(\text{Ma} + 1)]$ , and  $\omega_0$  is the angular frequencies of the incident acoustic wave.

Fig. 5 shows a quarter cross section of the acoustic pressure obtained as a simulation result for  $f=5700\text{Hz}$ ,  $\text{Ma}=0.15$ , and  $r_a=25\text{mm}$ . This figure shows that even in turbulent flow, sound transmission can be relatively blocked due to the geometry of the acoustic metamaterial. Thus, we investigated the sound transmission loss while increasing the flow velocity.

Fig. 6 and Fig. 7 show the sound transmission loss results calculated while changing the size of Ma and the number of annular cavities in the case of  $r_a=25\text{mm}$ . In order to evaluate the sound transmission loss corresponding to the flow velocity and the number of annular cavities in detail, in Fig. 6(a)-6(d) and Fig. 7(a)-7(c), the number of annular cavities was changed from 1 to 5 and the size of Ma was changed from 0.02 to 0.22. Also, in Fig. 7(d), a detailed calculation of the transmission loss graph is shown while changing the number of annular cavities from 1 to 7 when the flow velocity is  $\text{Ma} = 0.15$ .

In the case of  $\text{Ma}=0$  and  $r_a=25\text{mm}$ , the resonant frequency is 3804.8Hz. If you analyze Fig. 6(a) in detail, you can

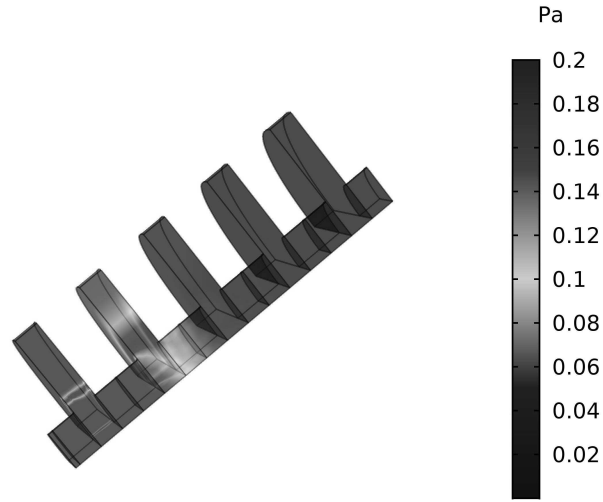


**Fig. 5 A quarter cross section of the acoustic pressure in the case of  $f=5700\text{Hz}$ ,  $\text{Ma}=0.15$ , and  $r_d=25\text{mm}$ .**

see that the resonance frequency is rather lower than in the case of no flow. In this case, since  $\text{Ma}=0.02$ , the convective velocity is small, on the contrary, the Kolomogorov's scale is very large (see Fig. 4). Therefore, the effect of eddy is greater than the effect of convective velocity on sound transmission. The fact that the resonance frequency in the case of  $N=1,2,3,4$  in Fig. 6(a) is lower than that in the case of no flow shows that the effect of eddy shifts the resonance frequency to a lower frequency. The figure also reflects the fact that as  $N$  increases, the intrinsic interaction of acoustic metamaterial becomes stronger, and the peak intensity gradually increases. When  $N=5$ , a series of changes occurs in the sound transmission loss values. After the first peak of  $3677.9\text{Hz}$  occurs, the values gradually change to the second peak of  $3938.3\text{Hz}$ , resulting in a widening of the resonance peak. When  $N=5$ , the number of annular cavities increases compared to  $N=1,2,3,4$ . Therefore, the interaction between the particle vibration in the sound propagation direction in the circular duct and the particle vibration perpendicular to the sound propagation direction in the annular cavity becomes strong. In this case, not only the effect of eddy, but also the intrinsic interaction of acoustic metamaterial has a considerable influence on the sound propagation. Of course, the fact that the largest peak frequency in the figure has been lowered to  $3677.9\text{Hz}$  shows that the eddy effect still plays a large role at this time. However, the newly revealed widening properties in the figure reflect that the intrinsic interaction of acoustic metamaterials has a significant effect on sound propagation. In the case of Fig. 6(b), as  $\text{Ma}$  increases, the effect of convection becomes larger than that in the case of  $\text{Ma}=0.02$ . This can be known well by seeing that the peak frequency shifted to  $3824.7\text{Hz}$  when  $\text{Ma}=0.05$  and  $N=5$ . However, in this case, the widening property is not significantly different from the case of  $\text{Ma}=0.02$ . In the case of Fig. 6(c), the effect of convection becomes stronger, and the widening property appears from  $N=4$ . In the case of  $\text{Ma} = 0.15$  and  $\text{Ma} = 0.17$ , the intrinsic interaction effect due to the geometry of the acoustic metamaterial, the effect

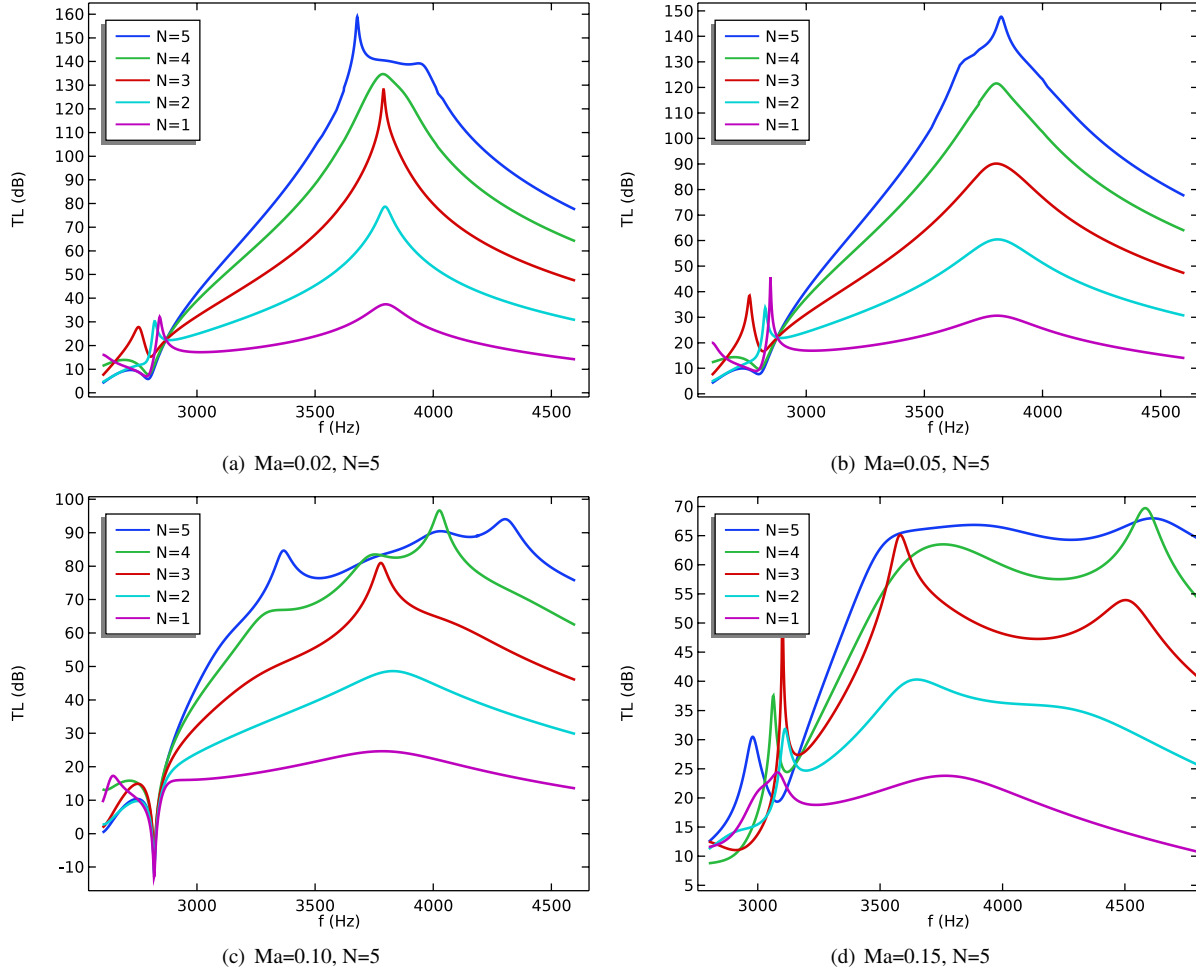


**Fig. 6 Sound transmission loss corresponding to the size of  $Ma$  and the number of annular cavities with  $r_a=25\text{mm}$  in the case of  $Ma=0.02, 0.05, 0.10,$  and  $0.15$ .**

of convection, and the effect of eddy become similar. As a result, in Fig. 6(d) and Fig 7(a), widening property appears from  $N=1$ . However, in the case of  $Ma = 0.17$ , the effect of convection was greater than in the case of  $Ma = 0.15$ , and the peak frequencies were shifted to a larger frequency. When  $Ma$  is continuously increased and  $Ma = 0.20, 0.22$  is reached, the effect of convection becomes much larger than the effect of eddy and the geometrical interaction effect of acoustic metamaterial, so the widening property does not appear and the peak frequency moves to a larger frequency (Figure 7(b),(c)). Fig. 7(d) is a graph that investigates the sound transmission loss while increasing the number of annular cavities in the velocity range of  $Ma = 0.15$  where the three interactions are similar. Fig. 7(d) shows that in the case of  $Ma = 0.15$ , the geometric interaction effect of acoustic metamaterial begins to play a leading role only when  $N$  is 7 or more.

Fig. 8 shows the sound pressure level results for the radii of the annular cavity when  $Ma = 0.15$ . In the case of  $Ma=0.15$ , it is affected by convection and eddy, but as in the case of  $Ma=0$ , as the radius increases, the resonance

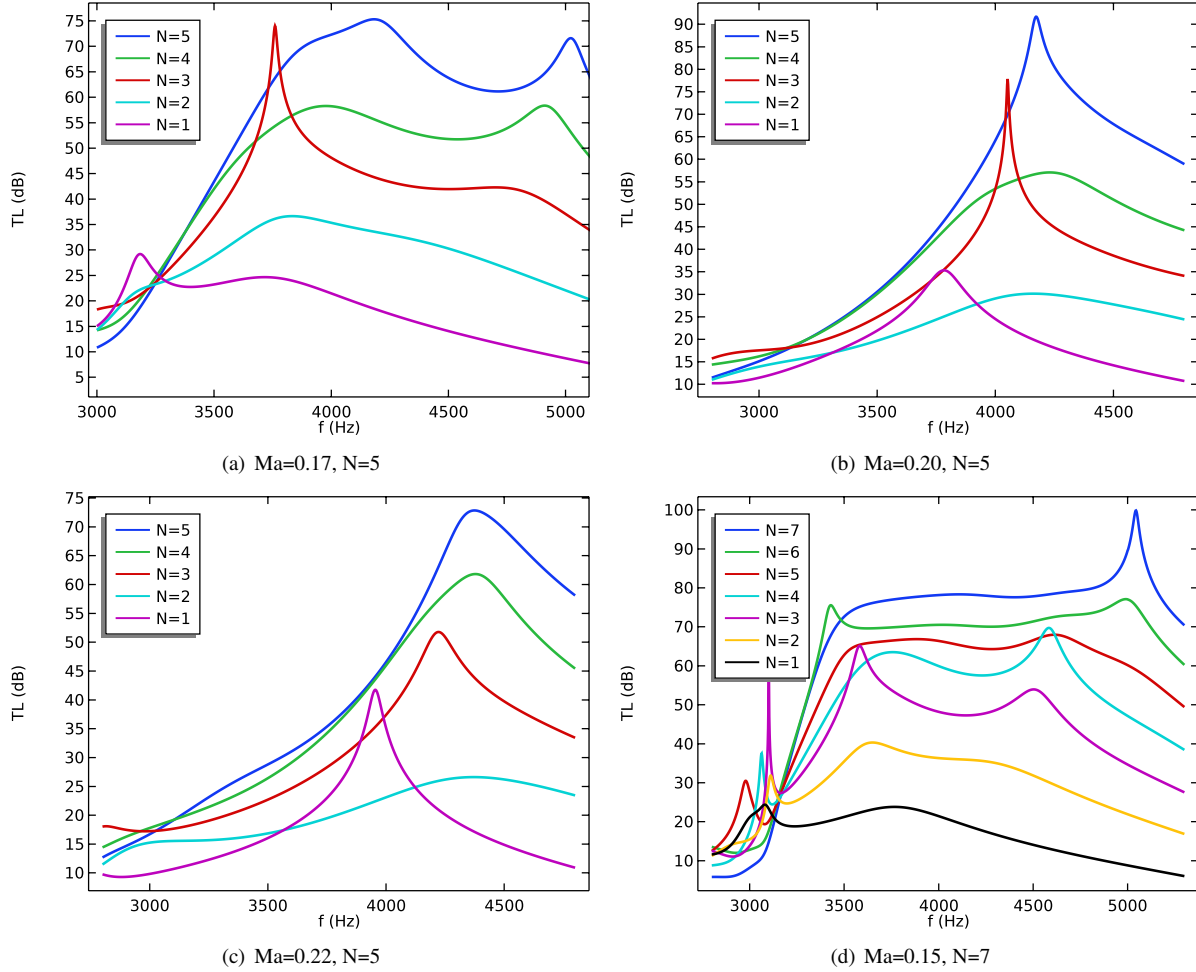


**Fig. 7** Sound transmission loss corresponding to the size of  $Ma$  and the number of annular cavities with  $r_a=25\text{mm}$  in the case of  $Ma=0.17, 0.20,$  and  $0.22$ . (\* (d) Transmission loss graph investigated while changing the number of annular cavities from 1 to 7 when  $Ma = 0.15$ )

frequency for the sound pressure level decreases. This fact shows that the particle vibration in the annular cavity analyzed when  $Ma = 0$  is a mechanism that cannot be ignored even in the acoustic propagation analysis with turbulent flow.

#### IV. Conclusion

In this study, we discussed the influence of the geometric structure, convection, and eddy on sound propagation in acoustic metamaterial with turbulent flow. First, in order to evaluate the influence of the geometric structure, the acoustic pressure of the acoustic metamaterial was investigated in the case of no flow. Looking at the sound pressure levels corresponding to the frequencies of the sound wave, it has resonance properties, and as the number of annular cavities increases, the resonance strength becomes stronger. Also, as the radius of the annular cavity increases, the resonant frequency decreases. This shows that the sound propagation properties of acoustic metamaterial are closely

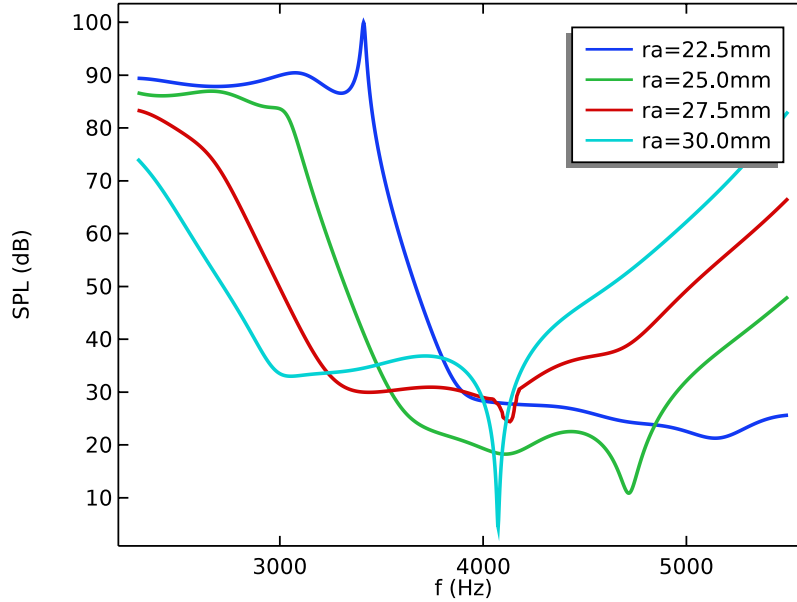


**Fig. 8 Sound pressure level results for the radii of annular cavity in case  $Ma = 0.15$ .**

related to the geometry.

To discuss the problem of sound propagation when turbulent flows into the acoustic metamaterial, not only the effect of convection and eddy, but also the effect of the intrinsic interactions reflecting the geometric structure of the acoustic metamaterial must be considered. Here, the intrinsic interaction refers to the interaction between the particle vibration in the sound propagation direction in the circular duct and the particle vibration perpendicular to the sound propagation direction in the annular cavity. It is not an easy matter to interpret this because all three effects contribute sound transmission. Of course, both convective and eddy effects reduce the intrinsic interaction of acoustic metamaterial in the circular duct, thus reducing the resonant peak intensity for sound transmission. However, considering that the direction of convection is the same as the direction of sound propagation and the direction of eddy is opposite to the direction of sound propagation, the effect of convective flow is opposite to that of eddy. In other words, the convection effect moves the resonance peak in the direction where the frequency is large, and the eddy effect moves the resonance peak in the direction where the frequency is low. However, when these are combined with the unique interaction properties of the acoustic metamaterial, the widening property of the resonance peak appears. In short, when all three effects cannot be ignored, competition phenomena appear with each other, and as a result, the resonance peak widens and the intensity decreases. In conclusion, the effects of convection, eddy, and intrinsic interactions arising from the unique geometry of acoustic metamaterial appear as the shift of the resonant frequency and the widening properties of the resonant peak.

By using the shift of the resonant frequency and the widening property of the resonant peak studied here, even when turbulence flows, it is possible to block noise by properly controlling the geometric size and shape of the acoustic



metamaterial. In particular, this can be used to block noise in transport systems such as train, car, and ship.

## Acknowledgments

It is a pleasure to thank Un Chol Ri, Yong Kwang Jong and Chol Su Ri for useful discussions. This work was supported by the National Program on Key Science Research of Democratic People's Republic of Korea (Grant No. 20-15-5).

## References

- [1] Brookea, D. C., Umnova, O., Leclaire, P., and Dupont, T., "Acoustic metamaterial for low frequency sound absorption in linear and nonlinear regimes," *Journal of Sound and Vibration*, Vol. 485, 2020, pp. 115585–115604. <https://doi.org/10.1016/j.jsv.2020.115585>.
- [2] Li, Y., and Assouar, B. M., "Acoustic metasurface-based perfect absorber with deep subwavelength thickness," *Applied Physics Letters*, Vol. 108, No. 6, 2016, pp. 063502–063505. <https://doi.org/10.1063/1.4941338>.
- [3] Gu, Z., Gao, H., Liu, T., Li, Y., and J., Z., "Dopant-modulated sound transmission with zero index acoustic metamaterials," *The Journal of the Acoustical Society of America*, Vol. 148, No. 3, 2020, pp. 1636–1641. <https://doi.org/10.1121/10.0001962>.
- [4] Qu, S., and Sheng, P., "Minimizing Indoor Sound Energy with Tunable Metamaterial Surfaces," *Physical Review Applied*, Vol. 14, No. 3, 2020, pp. 034060–034069. <https://doi.org/10.1103/PhysRevApplied.14.034060>.
- [5] Park, J. J., Park, C. M., Lee, K. J. B., and Lee, S. H., "Acoustic superlens using membrane-based metamaterials," *Applied Physics Letters*, Vol. 106, No. 5, 2015, pp. 051901–051904. <https://doi.org/10.1063/1.4907634>.
- [6] Zheng, M. Y., Park, C., Liu, X. N., Zhu, R., Hu, G. K., and Kim, Y. Y., "Non-resonant metasurface for broadband elastic wave mode splitting," *Applied Physics Letters*, Vol. 116, No. 17, 2020, pp. 171903–171907. <https://doi.org/10.1063/5.0005408>.
- [7] Lu, K., Wu, J., Guan, D., Gao, N., and Jing, L., "A lightweight low-frequency sound insulation membrane-type acoustic metamaterial," *AIP Advances*, Vol. 6, No. 2, 2016, pp. 025116–025125. <https://doi.org/10.1063/1.4942513>.
- [8] Fan, L., Chen, Z., Zhang, S., Ding, J., Li, X., and Zhang, H., "An acoustic metamaterial composed of multi-layer membrane-coated perforated plates for low-frequency sound insulation," *Applied Physics Letters*, Vol. 106, No. 15, 2015, pp. 151908–151912. <https://doi.org/10.1063/1.4918374>.
- [9] Wang, X., Zhao, H., Luo, X., and Huang, Z., "Membrane-constrained acoustic metamaterials for low frequency sound insulation," *Applied Physics Letters*, Vol. 108, No. 4, 2016, pp. 041905–041909. <https://doi.org/10.1063/1.4940717>.
- [10] Bok, E., Park, J. J., Choi, H., Han, C. K., Wright, O. B., and Lee, S. H., "Metasurface for Water-to-Air Sound Transmission," *Physical Review Letters*, Vol. 120, No. 4, 2018, pp. 044302–044307. <https://doi.org/10.1103/PhysRevLett.120.044302>.

- [11] Su, H., Zhou, X., Xu, X., and Hu, G., “Experimental study on acoustic subwavelength imaging of holey-structured metamaterials by resonant tunneling,” *The Journal of the Acoustical Society of America*, Vol. 135, No. 4, 2014, pp. 1686–1691. <https://doi.org/10.1121/1.4868395>.
- [12] Jiang, X., Li, Y., and Zhang, L. K., “Thermoviscous effects on sound transmission through a metasurface of hybrid resonances,” *The Journal of the Acoustical Society of America*, Vol. 141, No. 4, 2017, pp. EL363–EL368. <https://doi.org/10.1121/1.4979682>.
- [13] Sui, N., Yan, X., Huang, T. Y., Xu, J., Yuan, F. G., and Jing, Y., “A lightweight yet sound-proof honeycomb acoustic metamaterial,” *Applied Physics Letters*, Vol. 106, No. 17, 2015, pp. 171905–171908. <https://doi.org/10.1063/1.4919235>.
- [14] Jung, J. W., Kim, J. E., and Lee, J. W., “Acoustic metamaterial panel for both fluid passage and broadband sound-proofing in the audible frequency range,” *Applied Physics Letters*, Vol. 112, No. 4, 2018, pp. 041903–041907. <https://doi.org/10.1063/1.5004605>.
- [15] Yang, Z. J., Gao, F., Shi, X. H., Lin, X., Gao, Z., Chong, Y. D., and Zhang, B. L., “Topological Acoustics,” *Physical Review Letters*, Vol. 114, No. 11, 2015, pp. 114301–114304. <https://doi.org/10.1103/PhysRevLett.114.114301>.
- [16] Romani, G., Ye, Q. Q., Avallone, F., Ragni, D., and Casalino, D., “Numerical analysis of fan noise for the NOVA boundary-layer ingestion configuration,” *Aerospace Science and Technology*, Vol. 96, 2020, pp. 105532–105553. <https://doi.org/10.1016/j.ast.2019.105532>.
- [17] Nardini, M., Sandberg, R. D., and Schlanderer, S. C., “Computational study of the effect of structural compliance on the noise radiated from an elastic trailing-edge,” *Journal of Sound and Vibration*, Vol. 485, 2020, pp. 115533 –115559. <https://doi.org/10.1016/j.jsv.2020.115533>.
- [18] Kusano, K., Yamada, K., and Furukawa, M., “Aeroacoustic simulation of broadband sound generated from low-Mach-number flows using a lattice Boltzmann method,” *Journal of Sound and Vibration*, Vol. 467, 2020, pp. 115044–115061. <https://doi.org/10.1016/j.jsv.2019.115044>.
- [19] Yao, H., and Davidson, L., “Vibro-acoustics response of a simplified glass window excited by the turbulent wake of a quarter-spherocylinder body,” *The Journal of the Acoustical Society of America*, Vol. 145, No. 5, 2019, pp. 3163–3176. <https://doi.org/10.1121/1.5109548>.
- [20] Tang, H., Lei, Y. L., and Li, X. Z., “An Acoustic Source Model for Applications in Low Mach Number Turbulent Flows, Such as a Large-Scale Wind Turbine Blade,” *Energies*, Vol. 12, No. 23, 2019, pp. 4596–4613. <https://doi.org/10.3390/en12234596>.
- [21] Chaitanya, P., Joseph, P., and Ayton, L. J., “Leading edge profiles for the reduction of airfoil interaction noise,” *AIAA Journal*, Vol. 58, No. 3, 2020, pp. 1118–1129. <https://doi.org/10.2514/1.J058456>.
- [22] Miotto, R., Wolf, W., and de Santana, L., “Leading-Edge Noise Prediction of General Airfoil Profiles with Spanwise-Varying Inflow Conditions,” *AIAA Journal*, Vol. 56, No. 5, 2018, pp. 1711–1716. <https://doi.org/10.2514/1.J056716>.

- [23] Deuse, M., and Sandberg, R. D., “Different noise generation mechanisms of a controlled diffusion aerofoil and their dependence on Mach number,” *Journal of Sound and Vibration*, Vol. 476, 2020, pp. 115317–115335. <https://doi.org/10.1016/j.jsv.2020.115317>.
- [24] Ananthan, V., Bernicke, P., Akkermans, R., Hu, T., and Liu, P., “Effect of porous material on trailing edge sound sources of a lifting airfoil by zonal Overset-LES,” *Journal of Sound and Vibration*, Vol. 480, 2020, pp. 115386–115404. <https://doi.org/10.1016/j.jsv.2020.115386>.
- [25] Ostashev, V. E., and Wilson, D. K., *Acoustics in moving inhomogeneous media*, 2<sup>nd</sup> ed., Taylor and Francis, 2016, pp. 27–62.
- [26] Menter, F., “Two-Equation Eddy-Viscosity Turbulence Models for Engineering Applications,” *AIAA Journal*, Vol. 32, No. 8, 1994, pp. 1598–1605. <https://doi.org/10.2514/3.12149>.
- [27] Du, L., Holmberg, A., Karlsson, M., and Abom, M., “Sound amplification at a rectangular T-junction with merging mean flows,” *Journal of Sound and Vibration*, Vol. 367, 2016, pp. 69–83. <https://doi.org/10.1016/j.jsv.2015.12.042>.
- [28] Gikadi, J., Foeller, S., and Sattelmayer, T., “Impact of turbulence on the prediction of linear aeroacoustic interactions: Acoustic response of a turbulent shear layer,” *Journal of Sound and Vibration*, Vol. 333, No. 24, 2014, pp. 6548—6559. <https://doi.org/10.1016/j.jsv.2014.06.033>.
- [29] Pierce, A. D., *Acoustics (An Introduction to Its Physical Principles and Applications)*, 3<sup>rd</sup> ed., Springer, 2019, pp. 68, 69.
- [30] Kundu, P. K., Cohen, I. M., and Dowling, D., *Fluid Mechanics*, 5<sup>th</sup> ed., Elsevier, 2012, pp. 564–571.